Description of the dipole giant resonance in heavy and superheavy nuclei within Skyrme random-phase approximation

W. Kleinig,[1,2] V. O. Nesterenko,[1,*] J. Kvasil,[3] P.-G. Reinhard,[4] and P. Vesely[3]
[1]*Laboratory of Theoretical Physics, Joint Institute for Nuclear Research, Dubna, Moscow region, RU-141980, Russia*
[2]*Technische Universität Dresden, Inst. für Analysis, D-01062, Dresden, Germany*
[3]*Institute of Particle and Nuclear Physics, Charles University, CZ-18000, Praha 8, Czech Republic*
[4]*Institut für Theoretische Physik II, Universität Erlangen, D-91058, Erlangen, Germany*
(Received 30 May 2008; published 17 October 2008)

The $E1(T = 1)$ isovector dipole giant resonance (GDR) in heavy and superheavy deformed nuclei is analyzed over a sample of 18 rare-earth nuclei, four actinides, and three chains of superheavy elements ($Z = 102$, 114, and 120). The basis of the description is the self-consistent separable random-phase approximation (SRPA) using the Skyrme force SLy6. The model well reproduces the experimental data in the rare-earth and actinide regions. The trend of the resonance peak energies follows the estimates from collective models, showing a bias to the volume mode for the rare-earth isotopes and a mix of volume and surface modes for actinides and superheavy elements. The widths of the GDR are mainly determined by the Landau fragmentation, which in turn is found to be strongly influenced by deformation. A deformation splitting of the GDR can contribute to about one-third of the width, and about 1 MeV further broadening can be associated with mechanisms beyond the SRPA description (e.g., escape widths and coupling with complex configurations).

DOI: 10.1103/PhysRevC.78.044313 PACS number(s): 21.60.Jz, 24.30.Cz, 27.70.+q, 27.90.+b

I. INTRODUCTION

The isovector giant dipole resonance (GDR) is a most prominent and much studied excitation mode of nuclei; see, e.g., Refs. [1,2]. Nonetheless, it remains a subject of current interest as there are many aspects that deserve more detailed investigations such as photoexcitation cross sections in exotic nuclei, which play a role in astrophysical reaction chains [3], or isotopic trends of the GDR including the regimes of deformed nuclei. The present paper aims at a theoretical survey of the GDR in isotopic chains of heavy and superheavy nuclei.

The high importance of the GDR has triggered many theoretical surveys of nuclear collective motion, starting from a purely collective description [4,5] and then slowly establishing a link to microscopic models in the framework of the Random-Phase Approximation (RPA) [6,7]. The theoretical description has developed greatly over the years. The majority of RPA investigations in the past employed shell model potentials plus an effective residual interaction (Migdal theory) [8–10]. In the meantime, self-consistent nuclear models have been steadily improving toward a reliable description of nuclear structure and excitations; for reviews, see, e.g., Refs. [11–13]. These models belong to the class of density functional methods that aims at a universal energy functional from which all static and dynamics equations could be derived in a strictly variational frame [14,15]. Being rather universal by construction, such density functional models are promising for investigation in exotic areas, e.g., drip-line and superheavy nuclei. The studies in this paper are based on the Skyrme functional, which was introduced in Refs. [16,17] and extended to a dynamical description shortly afterward [18–20]. The performance of self-consistent RPA calculations using the Skyrme functional was tested systematically in Refs. [21,22], and it was found that one can have a reliable description when taking care to choose an appropriate parametrization.

Systematic scans through the isotopic landscape and the study of exotic nuclei run over many deformed nuclei. Fully fledged RPA calculations for deformed nuclei are feasible [23] but extremely time consuming and not suited for systematic investigations. Superheavy nuclei are especially demanding because of the coexistence of two obstacles: large size and deformation. Accurate but less demanding RPA techniques are needed. To that end, the separable RPA (SRPA) based on the Skyrme functional was recently developed [24–26]. The self-consistent factorization of the residual interaction in SRPA dramatically reduces the computational expense and so gives way to systematic explorations of nuclear giant resonances in both spherical and deformed nuclei [24–29]. In this paper, we concentrate on the isovector ($T = 1$) electric GDR.

As shown in our previous studies [24–29], SRPA provides an accurate description of the GDR in spherical and deformed nuclei. We obtained good agreement with experiment for ^{154}Sm, ^{238}U, and Nd isotopes with $A = 142$, 144, 146, 148, 150. Eight different Skyrme forces were checked in these investigations. In this paper, we aim at a large systematics over the isotopic landscape and decide on one parametrization, namely, SLy6 [30], which was found to provide a satisfying description of the GDR for spherical and deformed nuclei. In a first step, SRPA results for the GDR will be compared with all available experiment data in rare-earth and actinide regions. In particular, we consider nuclei ^{156,160}Gd, ^{166,168}Er, ^{170,172,174,176}Yb, ^{176,178,180}Hf, ^{182,184,186}W, ^{186,188,190,192}Os, ^{232}Th, and ^{234,236,238}U. Basic characteristics (energy centroid, width, deformation splitting) and their trends with system size will be analyzed.

In a second step, we will investigate the GDR in superheavy nuclei for the three isotopic chains: nobelium with

*nester@theor.jinr.ru

$Z = 102\,(A = 242, 248, 254, 262, 270)$, $Z = 114\,(A = 264, 274, 284, 294, 304)$, and $Z = 120\,(A = 280, 288, 294, 304, 312)$. As discussed below, this set covers most of the important mass regions and so is sufficiently representative. The main features of the GDR will be analyzed and compared with those in the rare-earth and actinide regions.

The paper is organized as follows. The calculation scheme, methods of analysis, and choice of the isotopes are sketched in Sec. II. In Sec. III the results of the calculations for the GDR in rare-earth, actinide, and superheavy nuclei are discussed. A summary is given in Sec. IV.

II. CALCULATION SCHEME

A. SRPA

The SRPA formalism is given elsewhere [24–26], so we present here only its principle points. The SRPA approximates the residual interaction of Skyrme RPA in factorized (separable) form as

$$\hat{V}^{\rm sep}_{\rm res} = -\frac{1}{2}\sum_{ss'}\sum_{k,k'=1}^{K}\{\kappa_{sk,s'k'}\hat{X}_{sk}\hat{X}_{s'k'} + \eta_{sk,s'k'}\hat{Y}_{sk}\hat{Y}_{s'k'}\}, \quad (1)$$

where the indices s and s' label neutrons and protons, k numbers the separable terms, $\hat{X}_{sk}$ and $\hat{Y}_{sk}$ are time-even and time-odd Hermitian one-body operators, $\kappa_{sk,s'k'}$ and $\eta_{sk,s'k'}$ are the corresponding strength matrices. We need these two kinds of operators because the relevant Skyrme functionals involve both time-even (nucleon ρ, kinetic τ, and spin-orbital $\mathcal{J}$) and time-odd (current $\vec{j}$, spin σ, and spin kinetic $\vec{T}$) densities, see Ref. [11].

The starting point is a Skyrme functional $E[J^\alpha_s(\vec{r},t)]$ with a set of local densities J^α_s being sorted by α. The separable operators and strength matrices are derived from the functional by using the scaling transformation for the perturbed wave function of the system:

$$|\Psi(t)\rangle_s = \prod_{k=1}^{K}\exp[-iq_{sk}(t)\hat{P}_{sk}]\exp[-ip_{sk}(t)\hat{Q}_{sk}]|\rangle_s, \quad (2)$$

where both $|\Psi(t)\rangle_s$ and ground state $|\rangle_s$ are Slater determinants, $\hat{Q}_{sk}(\vec{r})$ and $\hat{P}_{sk}(\vec{r}) = i[\hat{H},\hat{Q}_{sk}]$ are generalized coordinate (time-even) and momentum (time-odd) Hermitian one-body input operators, $\hat{H}$ stands for the full Hamiltonian. Further,

$$q_{sk}(t) = \bar{q}_{sk}\cos(\omega t), \qquad p_{sk}(t) = \bar{p}_{sk}\sin(\omega t) \quad (3)$$

are corresponding collective variables. The number K of input operators in Eq. (2) determines the number of separable terms in $\hat{V}^{\rm sep}_{\rm res}$. The treatment converges to exact RPA for $K\to\infty$. In practice, a good approximation to RPA can already be obtained for a small $K = 2$–5 if the generating operators $\hat{Q}_{sk}$ and $\hat{P}_{sk}$ are properly chosen; see Sec. II C and Refs. [24,25].

The separable operators and (inverse) strength matrices in Eq. (1) are constructed as [24–26]

$$\hat{X}_{sk} = \sum_{s'}\hat{X}^{s'}_{sk} = i\sum_{\alpha'\alpha s'}\frac{\delta^2 E}{\delta J^{\alpha'}_{s'}\delta J^{\alpha}_{s}}\langle[\hat{P}_{sk},\hat{J}^{\alpha}_{s}]\rangle\hat{J}^{\alpha'}_{s'}, \quad (4a)$$

$$\hat{Y}_{sk} = \sum_{s'}\hat{Y}^{s'}_{sk} = i\sum_{\alpha'\alpha s'}\frac{\delta^2 E}{\delta J^{\alpha'}_{s'}\delta J^{\alpha}_{s}}\langle[\hat{Q}_{sk},\hat{J}^{\alpha}_{s}]\rangle\hat{J}^{\alpha'}_{s'}, \quad (4b)$$

$$\kappa^{-1}_{s'k',sk} = \sum_{\alpha\alpha'}\frac{\delta^2 E}{\delta J^{\alpha'}_{s'}\delta J^{\alpha}_{s}}\langle[\hat{P}_{sk},\hat{J}^{\alpha}_{s}]\rangle\langle[\hat{P}_{s'k'},\hat{J}^{\alpha'}_{s'}]\rangle, \quad (5a)$$

$$\eta^{-1}_{s'k',sk} = \sum_{\alpha\alpha'}\frac{\delta^2 E}{\delta J^{\alpha'}_{s'}\delta J^{\alpha}_{s}}\langle[\hat{Q}_{sk},\hat{J}^{\alpha}_{s}]\rangle\langle[\hat{Q}_{s'k'},\hat{J}^{\alpha'}_{s'}]\rangle, \quad (5b)$$

where $\hat{J}^\alpha_s$ are the operators associated with the densities J^α_s. As seen from Eqs. (4) and (5), the separable ansatz (1) explores the residual interaction of the Skyrme functional through the second functional derivatives.

The final RPA equations have the form [24–26]

$$\sum_{sk}\{\bar{q}^\nu_{sk}[F^{(XX)}_{s'k',sk} - \kappa^{-1}_{s'k',sk}] + \bar{p}^\nu_{sk}F^{(XY)}_{s'k',sk}\} = 0, \quad (6a)$$

$$\sum_{sk}\{\bar{q}^\nu_{sk}F^{(YX)}_{s'k',sk} + \bar{p}^\nu_{sk}[F^{(YY)}_{s'k',sk} - \eta^{-1}_{s'k',sk}]\} = 0, \quad (6b)$$

with

$$F^{(AB)}_{s'k',sk} = 2\sum_{s'',ph\in s''}\alpha_{AB}\frac{\langle ph|\hat{A}^{s''}_{sk}|\rangle^*\langle ph|\hat{B}^{s''}_{s'k'}|\rangle}{\varepsilon^2_{ph} - \omega^2_\nu}, \quad (7)$$

and

$$\alpha_{AB} = \begin{pmatrix} \varepsilon_{ph}, & \text{for } \hat{A} = \hat{B} \\ -i\omega_\nu, & \text{for } \hat{A} = \hat{Y}, \hat{B} = \hat{X} \\ i\omega_\nu, & \text{for } \hat{A} = \hat{X}, \hat{B} = \hat{Y} \end{pmatrix}. \quad (8)$$

Here $\langle ph|\hat{A}^{s''}_{s'k'}|\rangle$ is the matrix element for the two-quasiparticle state $|ph\rangle$, ε_{ph} is the energy of this state, ω_ν is the energy of the RPA state $|\nu\rangle$. The amplitudes of the RPA phonon operator

$$\hat{C}^\dagger_\nu = \sum_s\sum_{ph\in s}\left(c^{\nu-}_{ph}\hat{A}^\dagger_{ph} - c^{\nu+}_{ph}\hat{A}_{ph}\right) \quad (9)$$

are determined via solutions of Eqs. (6a) and (6b) as

$$c^{\nu\pm}_{ph\in s} = -\sum_{s'k'}\frac{\bar{q}^\nu_{s'k'}\langle ph|\hat{X}^s_{s'k'}\rangle \mp i\,\bar{p}^\nu_{s'k'}\langle ph|\hat{Y}^s_{s'k'}\rangle}{2(\varepsilon_{ph}\pm\omega_\nu)}, \quad (10)$$

where $\hat{A}^\dagger_{ph}$ and $\hat{A}_{ph}$ are operators of creation and destruction of two-quasiparticle states.

SRPA equations presented above are obtained for arbitrary functionals $E[J^\alpha_s(\vec{r},t)]$, including Skyrme ones, see details in Refs. [24–26]. The model is self-consistent in the sense that both the static mean field

$$\hat{h}_0 = \sum_{\alpha s}\frac{\delta E}{\delta J^\alpha_s}\hat{J}^\alpha_s \quad (11)$$

and the residual interaction of Eqs. (1), (4) and (5) are derived from the same functional. The rank of the RPA matrix (6) is determined by the number K of the input operators in Eq. (2). Usually $K = 2$–5 [24–29], so the rank is very small. This drastically simplifies the RPA computational effort and allows us to perform systematic explorations even for heavy deformed nuclei.

B. SRPA strength function

Giant resonances in heavy deformed nuclei are formed by thousands of RPA states whose detailed contributions cannot be resolved experimentally. Then, instead of the solution of Eqs. (6), a direct computation of the strength function is more efficient and reasonable. For an external electric field of multipolarity $E1\mu$, the energy-weighted isovector dipole strength function reads

$$S(E1\mu;\omega) = \sum_{\nu} \omega_\nu \left|\langle \nu | \hat{f}_{E1\mu} | \rangle\right|^2 \zeta(\omega-\omega_\nu) = \Im\left[\frac{z^L \sum_{\beta\beta'} F_{\beta\beta'}(z) D_\beta(z) D_{\beta'}(z)}{\pi F(z)}\right]_{z=\omega+i\Delta/2} + \sum_s \sum_{ph\in s} \varepsilon_{ph} \left\langle ph \left| \hat{f}_{E1\mu} \right| \right\rangle^2 \zeta(\omega-\varepsilon_{ph}), \quad (12)$$

where $\beta = sk\tau$ with τ being the time parity, $\Im$ means the imaginary part of the value inside the brackets, $F(z)$ is the determinant of the RPA matrix (6) with ω_ν replaced by the complex argument z, $F_{\beta\beta'}(z)$ is the algebraic supplement of the determinant, and

$$D^{(X)}_{sk}(z) = \sum_{s'} \sum_{ph\in s'} \frac{\varepsilon_{ph} \langle ph | X^{s'}_{sk} | \rangle \langle ph | \hat{f}_{E1\mu} | \rangle}{\varepsilon^2_{ph} - z^2}, \quad (13a)$$

$$D^{(Y)}_{sk}(z) = i \sum_{s'} \sum_{ph\in s'} \frac{\omega_\nu \left\langle ph \left| Y^{s'}_{sk} \right| \right\rangle \left\langle ph \left| \hat{f}_{E1\mu} \right| \right\rangle}{\varepsilon^2_{ph} - z^2}. \quad (13b)$$

Further,

$$\hat{f}_{E1\mu} = \frac{N}{A} \sum_{p=1}^{Z} r_p Y_{1\mu}(\Omega_p) - \frac{Z}{A} \sum_{n=1}^{N} r_n Y_{1\mu}(\Omega_n) \quad (14)$$

is the operator of the dipole transition; N, Z, and A are neutron, proton, and mass numbers. The strength function (12) is smoothed by the Lorentz function

$$\zeta(\omega-\omega_\nu) = \frac{1}{2\pi} \frac{\Delta}{(\omega-\omega_\nu)^2 + \frac{\Delta^2}{4}}, \quad (15)$$

with the averaging parameter $\Delta = 2$ MeV in most of the calculations. Such averaging was found to be optimal for the comparison with experiment and simulation of broadening effects beyond SRPA, namely, escape widths and coupling with complex configurations (collisional broadening). The broadening through Landau fragmentation is already included in SRPA. In fact, escape width could also be covered by SRPA when working with absorbing or open boundary conditions. This, however, would make calculations an order of magnitude more involved without adding much information for our purposes here.

The total strength function is counted as a sum of its $\mu = 0$ and 1 branches [Eq. (12)]: $S(E1) = S(E10) + S(E11)$.

C. Details of calculations

The calculations were performed with the Skyrme force SLy6 [30], which had been proved to give a satisfying description of the GDR for heavy nuclei [25,27–29]. The residual interaction involves the contributions from (i) the time-even densities ρ, τ, and $\mathcal{J}$ and time-odd current $\vec{j}$, (ii) the direct and exchange (in the Slater approximation) Coulomb terms, (iii) the monopole pairing delta forces [25,26]. The latter are incorporated through the particle-particle pairing channel at the BCS level [25,26] (though the pairing impact on GDR was found to be weak). Further, the calculations employ a cylindrical coordinate-space grid with the mesh size 0.7 fm. The calculation box has 24–35 mesh points depending on the nuclear size and deformation.

The SRPA formalism itself does not provide the input operators $\hat{Q}_{sk}(\vec{r})$ in the scaling transformation (2). At the same time, their choice is crucial to converging the approximate residual interaction $\hat{V}^{\rm sep}_{\rm res}$ to the true Skyrme one with a minimal number of separable terms. We achieve this aim by using $\hat{Q}_{sk}(\vec{r})$ inputs which compel the separable operators $\hat{X}_{sk}(\vec{r})$ and $\hat{Y}_{sk}(\vec{r})$ to have maxima in different spatial regions of the nucleus, both in the surface and interior. As shown in Refs. [24,25], this way indeed allows one to obtain good convergence already with a few separable terms. The physical arguments suggest that the leading scaling operator $\hat{Q}_{s1}(\vec{r})$ should have the form of the applied external field in the long-wave approximation. The corresponding operators (4) are then most sensitive to the surface of the system. The next input operators are chosen to shift the maxima of operators (4), and hence the sensitivity, more and more to the interior [24,25]. Following this prescription, the present calculations use four input dipole operators $R_k(r)(Y_{1\mu} + \text{h.c.})$ with radial dependencies $R_1(r) = r$, $R_{k=2,3,4}(r) = j(q_k r)$, and q_k taken from Ref. [24]. Besides, the operator $r^3(Y_{3\mu} + \text{h.c.})$ is added to take into account the multipole mixing of excitations with the same projection μ and space parity π.

For all nuclei, the equilibrium quadrupole deformations are found by minimization of the total energy. The deformations are characterized by the charge quadrupole moments Q_2 and related dimensionless parameters β_2 as

$$Q_2 = \int d\vec{r} \rho_p(\vec{r}) r^2 Y_{20}, \quad \beta_2 = \sqrt{\frac{\pi}{5}} \frac{Q_2}{Z\langle r^2\rangle_p}, \quad (16)$$

where $\rho_p(\vec{r})$ is the proton density in the ground state, $\langle r^2\rangle_p = \int d\vec{r} \rho_p(\vec{r}) r^2/Z$ is the r.m.s. proton radius.

The calculations use a large single-particle basis resulting in two-quasiparticle dipole states up to ~65 MeV, see Table I.

TABLE I. Characteristics of the configuration space used in the calculations: minimal $E_{\rm min}$ and maximal $E_{\rm max}$ single-particle energies, number of the single-particle levels M for protons and neutrons, number of two-quasiparticle dipole states $N_{\rm 2qp}$ (for branches $\mu = 0$ and 1 altogether). See text for more details.

Nucleus	$E_{\rm min}$, $E_{\rm max}$ (MeV)		M		$N_{\rm 2qp}$
	Z	N	Z	N	
^{154}Gd	−45.4, +20.2	−57.2, +17.0	252	308	4720
^{238}U	−42.7, +19.3	−58.0, +14.8	307	393	6860
^{294}120	−36.4, +20.9	−58.7, +14.1	360	426	8720

The energy-weighted sum rule

$$\mathrm{EWSR}(T=1,\lambda=1)=9\frac{(\hbar e)^2}{8\pi m_1^*}\frac{NZ}{A} \tag{17}$$

is then exhausted by 92–95%. This sum rule includes the isovector effective mass m_1^*, because the velocity-dependent terms are involved; see discussion in Ref. [29]. In SLy6 we have actually $m_1^*/m=0.80$.

Since SRPA includes the dipole momentum-like input operators $\hat{P}=i[\hat{H},\hat{Q}]$, the spurious isoscalar dipole state should be automatically placed at zero energy [24]. And indeed in our calculations, the spurious strength is downshifted to an energy of 2–3 MeV, thus fully leaving the GDR region. Because of some natural computational limits (finite computational box, restricted single-particle basis), the spurious peak does not yet achieve the zero energy. Of course, this could be done for the price of a considerable increase of the box and basis, but then the calculations of GR in heavy deformed nuclei would need an impressive computational effort. We do not follow that path, since the spurious strength already resides safely below the GDR and the basis is enough to exhaust most of the sum rule (17).

To estimate the resonance energy centroid E, width Γ, and deformation splitting ΔE, the following prescriptions are applied. To determine E, the energy interval around the resonance with the strength larger than 10% of the maximal value is used, and the centroid of the strength inside this interval is determined. The same method is implemented to find centroids E_0 and E_1 of $\mu=0$ and 1 branches separately. Then the deformation splitting $\Delta E=E_1-E_0$ is obtained. The width Γ is determined at a half-maximum of the resonance.

SRPA does not take into account some important broadening mechanisms (e.g., escape widths, coupling with complex configurations), so we do not pretend to describe the full GDR widths. Instead, we simulate the experimental widths by sufficiently large Lorentz averaging ($\Delta=2$ MeV). Such simulation is also useful. Indeed SRPA can properly describe the Landau fragmentation and deformation splitting. So, subtracting these contributions from the simulated width, one can estimate the relative role of the remaining width mechanisms.

The experimental data for the GDR [31–40] include photoabsorption

$$\sigma=(\gamma,n)+(\gamma,p)+(\gamma,np)+(\gamma,2n)+(\gamma,d)+\cdots+(\gamma,f),$$

neutron yield

$$\sigma=(\gamma,n)+(\gamma,np)+2(\gamma,2n)+3(\gamma,3n)+\cdots+(\gamma,f),$$

and neutron product

$$\sigma=(\gamma,n)+(\gamma,np)+(\gamma,2n)+(\gamma,3n)+\cdots+(\gamma,f).$$

The photoabsorption data are preferable as they involve all the main decay channels and so most correspond to the strength function (12). If the photoabsorption data are absent, the neutron yield and neutron product can also be used for a rough comparison, since these data include most of the main channels. However, one should take into account that both neutron yield and product omit the (γ,p) channel and so can underestimate the strength and change the resonance gross structure. Besides, the neutron yield amplifies the neutron contributions $(\gamma,2n),(\gamma,3n),\ldots$, and hence the right wing of the resonance.

In what follows, we use experimental data for photoabsorption in ^{156}Gd [32], ^{160}Gd [33], ^{168}Er [32], ^{174}Yb [32], ^{178,180}Hf [32], ^{182,184,186}W [32], ^{232}Th [38], and ^{238}U [38]; neutron yield in ^{170,172,176}Yb [35] and ^{186,188,190,192}Os [37]; and neutron products $(\gamma,n)+(\gamma,np)+(\gamma,2n)$ in ^{166}Er [34] and ^{176}Hf [36] and $(\gamma,n)+(\gamma,np)+(\gamma,2n)+(\gamma,f)$ in ^{234}U [39] and ^{236}U [40].

In rare-earth and actinide regions, we consider all nuclei for which reasonable GDR experimental data exist (with the exception of Nd and Sm isotopes already explored in our previous papers [25,27–29]). In superheavy nuclei, we look at three isotopic chains: nobelium $Z=102$ ($A=242,248,254,262,270$), $Z=114$ ($A=264,274,284,294,304$), and $Z=120$ ($A=280,288,294,304,312$). As can be seen from Ref. [41], these chains cover the most interesting mass and deformation regions. Indeed, they involve the onset ($Z=102$), the center ($Z=114$), and the upper end ($Z=120$) of the superheavy region. Every chain extends through the whole neutron interval at a given Z. Different deformation regions are covered. For $Z=102$, we deal with well-deformed nuclei and small variation of the quadrupole deformation. The chains $Z=114$ and 120 show strong variations of the deformation with its decrease, when moving toward the magic neutron number $N=184$ [42]. The proton numbers $Z=114$ and 120 are tentatively magic [11,43] such that neutron shell structure acquires a decisive weight for sphericity or deformation.

III. RESULTS AND DISCUSSION

A. Rare-earth and actinide nuclei

Results of SRPA calculations for rare-earth and actinide nuclei are presented in Figs. 1–6. Note that for reasons of comparison the calculated strength function is rescaled to correspond roughly to the maximal magnitude of the experimental cross section. Moreover, because of the insufficient accuracy of the model and experimental resolution (see discussion in the previous section), we skip here the analysis of the fine structure that manifests itself mainly at the top of the resonance. The main attention will be paid to the resonance energy centroids and widths.

Figures 1 and 2 show an excellent agreement with experiment for Gd, Er, and Yb isotopes. The agreement is less perfect for Hf, W, and Os shown in Figs. 3 and 4: the calculated strength exhibits a slight (~0.5 MeV) downshift in Hf and W and a larger (~1 MeV) upshift in Os. It is known that Os isotopes are soft to oblate quadrupole deformation, which is confirmed by our calculations. However, as we checked, SRPA calculations on top of the oblate isomer do not improve agreement with the experiment. The discrepancies for Os may be partly caused by using the neutron yield experimental data. As discussed above, the neutron yield alone can amplify the right GDR flank, thus resulting in some apparent upshift

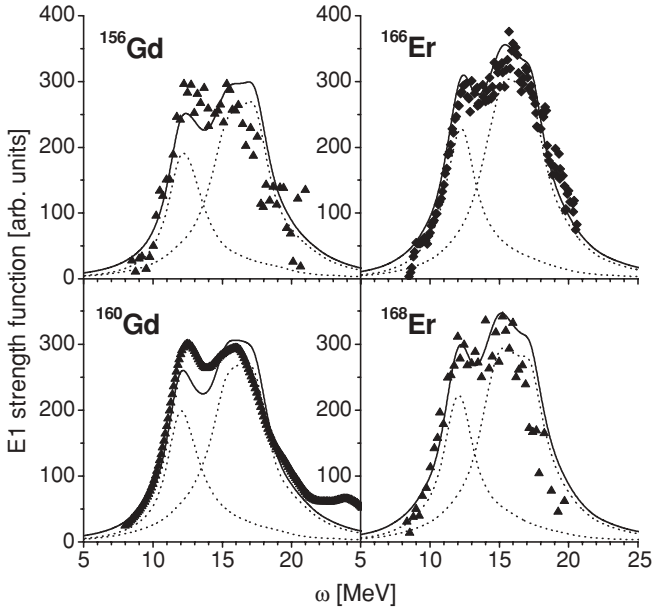

FIG. 1. Isovector dipole strength in ^{156,160}Gd and ^{166,168}Er. The calculated strength (solid curve) is compared with the experimental data for total photoabsorption [32,33] (triangles) and neutron product [34] (rhombs). Dotted curves represent the branches of the resonance with $\mu = 0$ (left small) and $\mu = 1$ (right large). The deformations are $\beta_2 = 0.347$, 0.359 and 0.348, 0.353, respectively.

relative to the total photoabsorption cross section. Results for the actinides in Fig. 5 also look encouraging. Modest deviations in the gross structure of ^{234,236}U can be explained by using the neutron product experimental data.

It is worth noting that the comprehensive analysis of experimental data reveals noticeable (sometimes significant) deviations in GDR measurements of different experimental groups [44]. Taking into account these uncertainties in the data, one may consider the agreement with experimental data

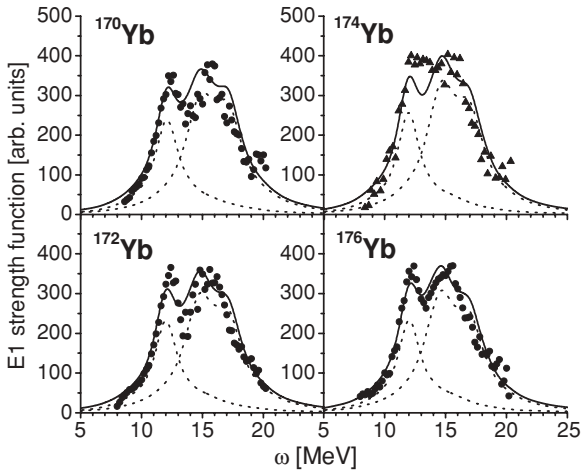

FIG. 2. Same as in Fig. 1, but for ^{170,172,174,176}Yb. The experimental data are for neutron yield [35] (solid circles) and total photoabsorption [32] (triangles). The deformation parameters are $\beta_2 = 0.350$, 0.347, 0.340, 0.327, respectively.

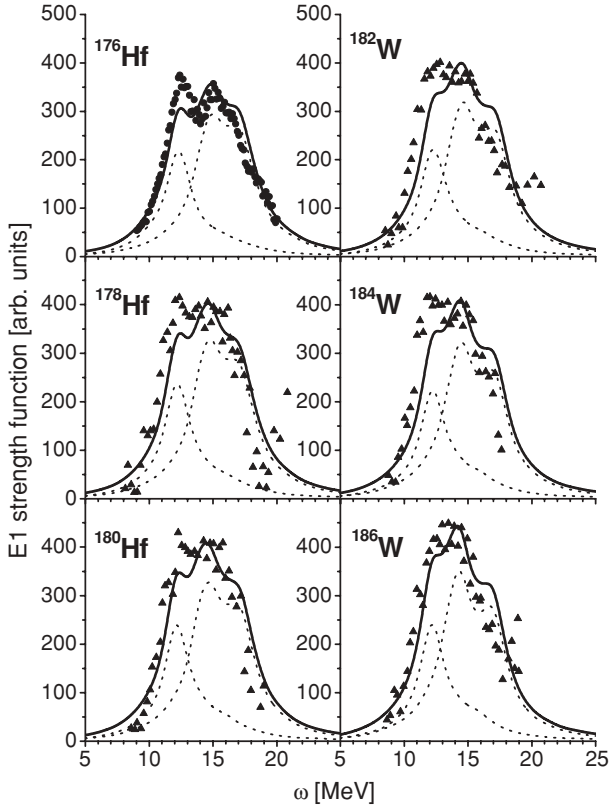

FIG. 3. Same as in Fig. 1, but for ^{176,178,180}Hf and ^{182,184,186}W. The experimental data are for total photoabsorption [32] (triangles) and neutron product [36] (solid circles). The deformation parameters for ^{176,178,180}Hf and ^{182,184,186}W are $\beta_2 = 0.330$, 0.296, 0.287 and 0.260, 0.252, 0.247, respectively.

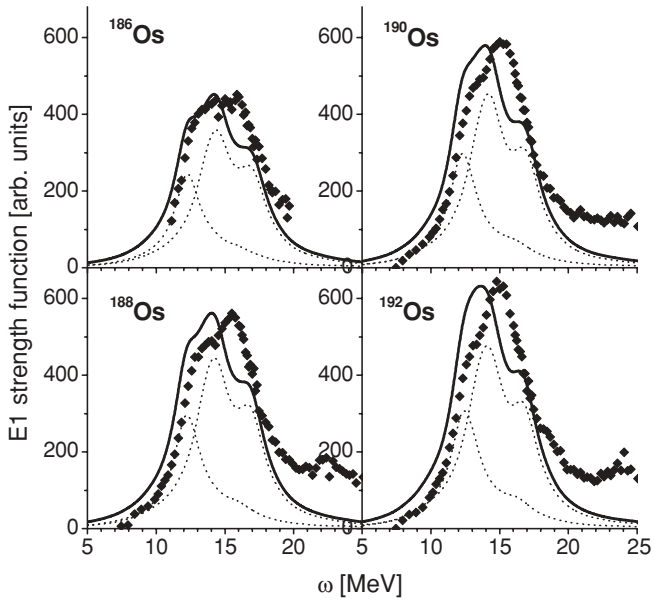

FIG. 4. Same as in Fig. 1, but for ^{186,188,190,192}Os. The experimental data are for neutron yield [37]. The deformation parameters are $\beta_2 = 0.222$, 0.217, 0.195, 0.172, respectively.

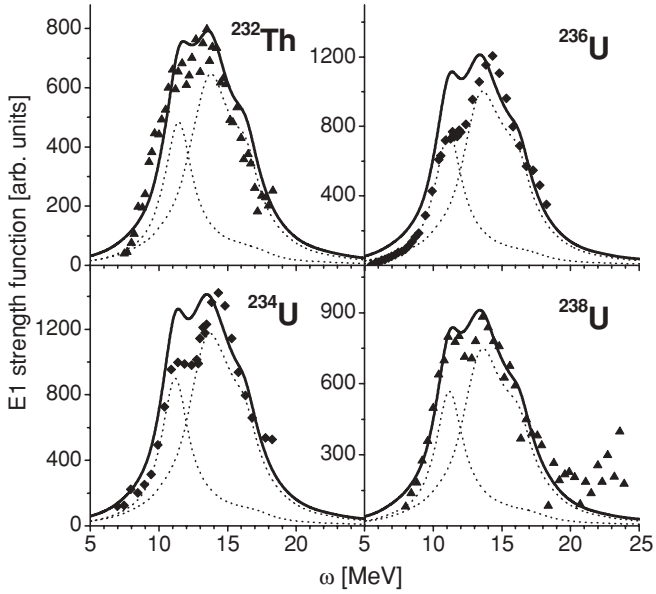

FIG. 5. Same as in Fig. 1, but for ^{232}Th and ^{234,236,238}U. The experimental data are for total photoabsorption [38] (triangles) and neutron product [39,40] (rhombs). The deformation parameters for ^{232}Th and ^{234,236,238}U are $\beta_2 = 0.256$ and 0.279, 0.286, 0.287, respectively.

as very satisfying, at least for energy centroids and widths (the latter is partly due to the large averaging $\Delta = 2$ MeV).

The correlation of the quadrupole moments of Eq. (16) with some resonance characteristics (width Γ, deformation splitting ΔE, energy centroid E) and trends of these characteristics with the mass number A are shown in Fig. 6. All nuclei in the sample have a significant quadrupole deformation. The calculated quadrupole moments are in excellent agreement with the experiment [45]. In the rare-earth nuclei, the moments have a maximum in the middle of the region. Note that the dimensionless deformation parameters β_2 as indicated in the captions of the previous figures are maximal at the onset of the region. The difference between Q_2 and β_2 maxima is related to the nuclear mass factor in Eq. (16). The direct contribution of the deformation splitting ΔE to the GDR width is maximal ($\sim$40%) in the first half of the region ($A < 176$) and then slowly decreases to 37–34% for Hf, 34–31% for W, and 31–24% for Os. Furthermore, ΔE is a bit increased in the actinides, where it reaches 30–33%. This trend obviously correlates with β_2. See also discussion of the GDR width and structure in Sec. III C.

In Fig. 6 (lower panel), the resonance energy is compared with empirical estimates based on Steinwedel-Jensen (SJ) [5]

$$E_{\mathrm{SJ}} = 81 A^{-1/3}\ \mathrm{MeV} \tag{18}$$

and Berman-Fultz (BF) [1,2]

$$E_{\mathrm{BF}} = (31.2 A^{-1/3} + 20.6 A^{-1/6})\ \mathrm{MeV} \tag{19}$$

collective models. BF takes into account both volume and surface contributions and treats the dipole resonance as a combination of Steinwedel-Jensen [5] and Goldhaber-Teller (GT) [4] scenarios. The calculated energies are closer to the SJ estimate [Eq. (18)] in the rare-earth region and to the BF estimate [Eq. (19)] in actinides. As shown below, the BF estimate is also more appropriate in superheavy nuclei. This agrees with the commonly accepted view that in heavy nuclei neither the density gradient ($\sim A^{-1/3}$) nor the nuclear surface impact ($\sim A^{-1/6}$) dominate the restoring force [2,46,47].

B. Superheavy nuclei

The agreement of SRPA results with the experimental data in rare-earth and actinide nuclei encourages its further application to superheavy nuclei. SRPA results for superheavy nuclei are exhibited in Figs. 7–10.

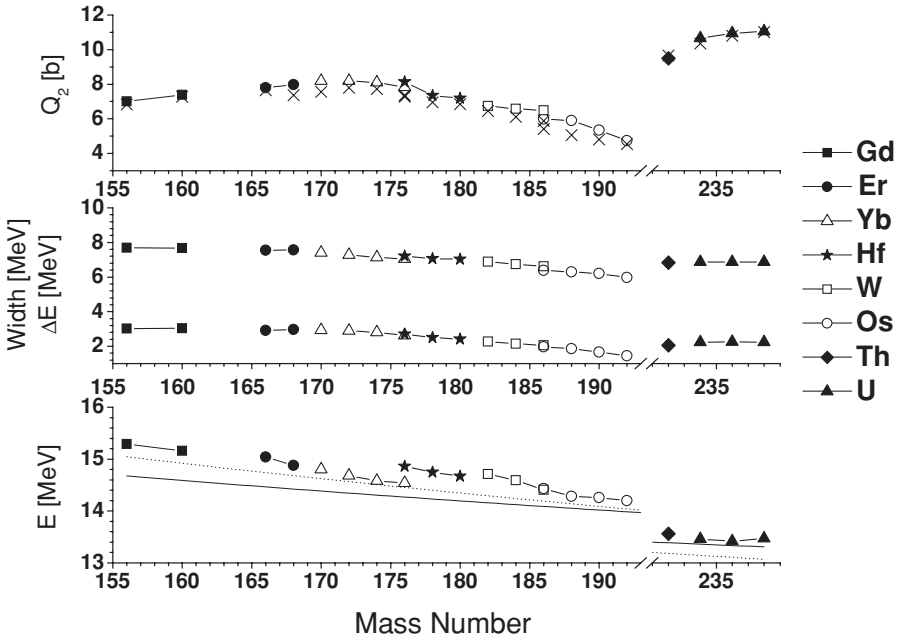

FIG. 6. Calculated characteristics of rare-earth and actinide nuclei as functions of mass number. Upper panel: quadrupole moments Q_2 compared with experimental values (crosses) [45]. Middle panel: widths Γ (upper set) and deformation splittings ΔE (lower set). Lower panel: energy centroids compared with the estimates of Eqs. (18) (dotted curve) and (19) (solid curve).

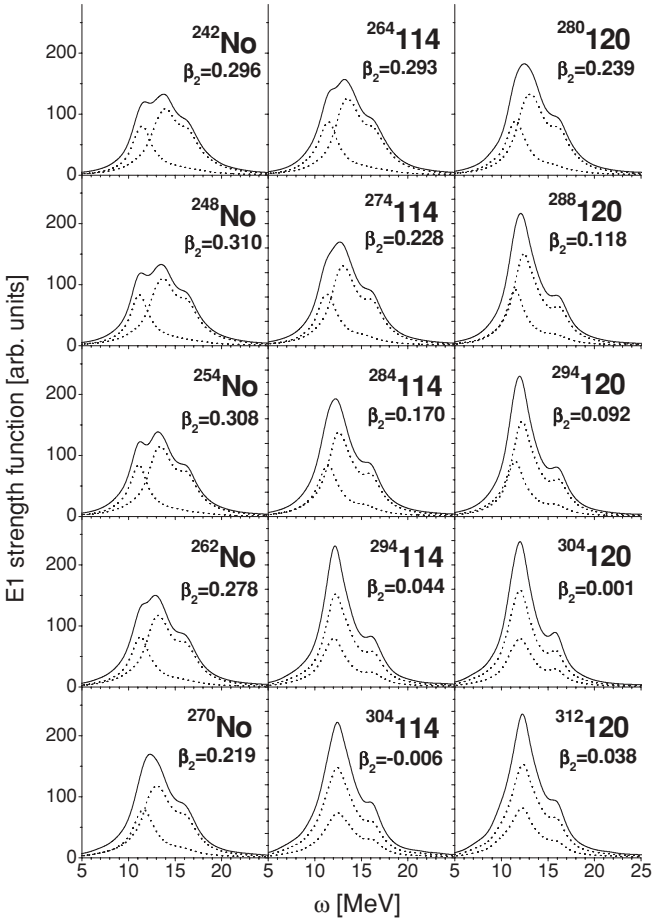

FIG. 7. Same as in Fig. 1, but for isotopes of superheavy nuclei No and $Z = 114$ and 120. The dimensionless proton quadrupole deformation β_2 is indicated in the plots.

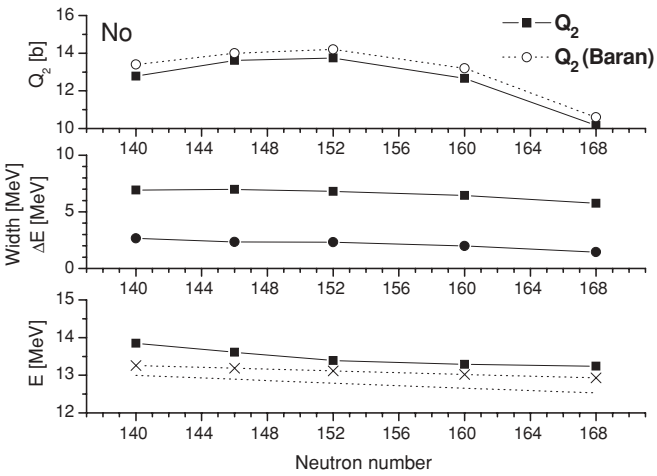

FIG. 8. Calculated characteristics of No isotopes as a function of their neutron number. Upper panel: quadrupole moments Q_2 (squares) compared with values from Ref. [41] (open circles). Middle panel: widths Γ (squares) and deformation splittings ΔE (solid circles). Lower panel: energy centroids (squares) compared with the estimates E_{SJ} [Eq. (18)] (dotted curve) and E_{BF} [Eq. (19)] (dotted curve with crosses).

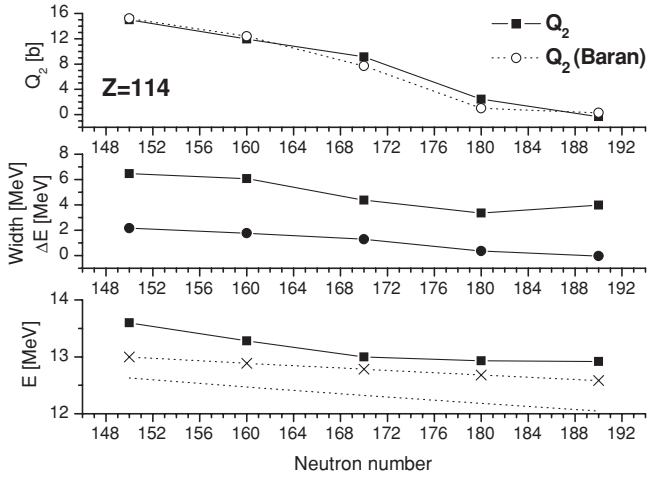

FIG. 9. Same as in Fig. 8, but for $Z = 114$ isotopes.

Figure 7 indicates that the GDR in this region is generally similar to that in rare-earth and actinide nuclei. In particular, the resonance width correlates with the quadrupole parameter β_2. Furthermore, the middle panels in Figs. 8–10 show that the direct contribution of the deformation splitting ΔE to the GDR width Γ does not exceed 40%, as in rare-earth and actinide nuclei. Note that our quadrupole moments Q_2 from the self-consistent calculations agree nicely with the values obtained within the macroscopic-microscopic model [41], see the upper panels in Figs. 8–10. The agreement persists even in mass regions with large variations of deformation.

At the same time, the GDR in superheavy nuclei shows some peculiarities. First, unlike the rare-earth nuclei, its energy is much closer to the BF estimate of Eq. (19) than to the SJ [Eq. (18)], which supports once again the treatment of the GDR in heavy nuclei as a mixture of SJ and GT modes. Maximal deviations from both estimates emerge at the ends of the isotopic chains, which is natural since these estimates do not parametrize any isospin dependence. Second, as seen from Figs. 8–10, the decrease of the resonance energies with neutron number N levels off and is even reversed to an increase at the

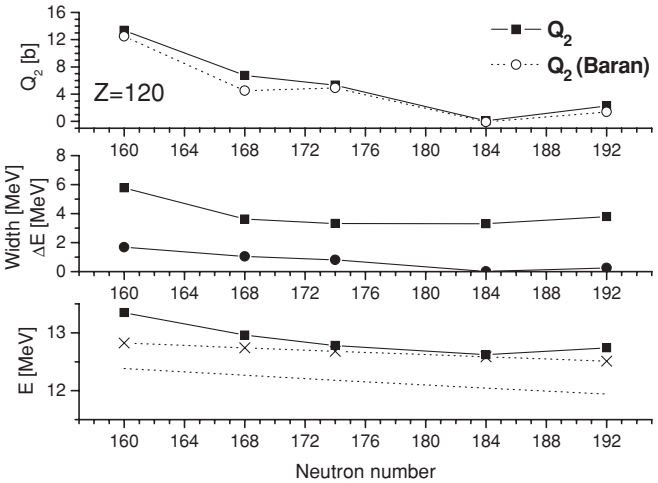

FIG. 10. Same as in Fig. 8, but for $Z = 120$ isotopes.

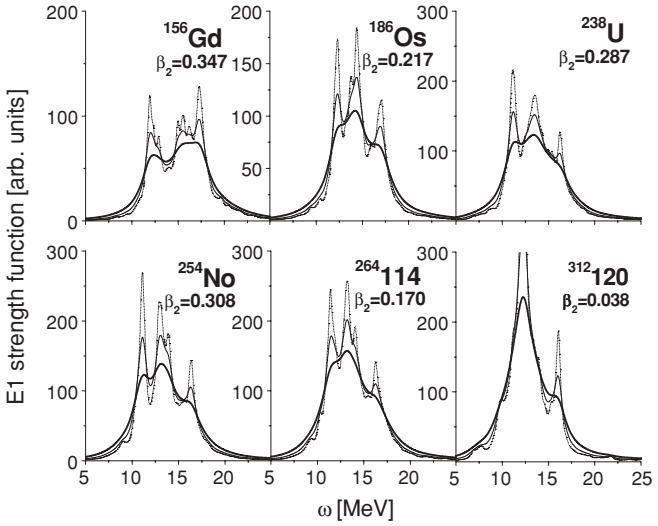

FIG. 11. Isovector dipole strength calculated with different averaging in the strength function (12): $\Delta = 0.5$ MeV (dash curve), 1 MeV (thin solid curve), and 2 MeV (bold solid curve). The parameters of the proton quadrupole deformation are given for each nucleus.

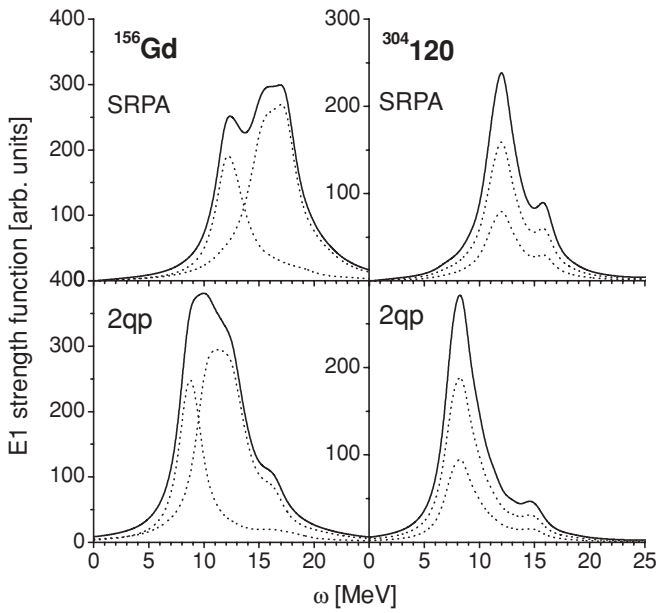

FIG. 12. Isovector dipole strength calculated with smoothing $\Delta = 2$ MeV in deformed ^{156}Gd and spherical ^{304}120. The upper panels show full SRPA results (with residual interaction) and the lower panels pure two-quasiparticle (2qp) strengths (without residual interaction). The separate branches $\mu = 0$ (small) and $\mu = 1$ (large) are plotted by the dotted line and their sum by the full line.

end of every isotope chain. A possible explanation may come from the increase of the symmetry energy $E_{\rm sym} = a_{\rm sym}(N - Z)^2/A^2$ (which is believed to be proportional to GDR energy ω [10]) at these neutron-rich edges. Note that such a turnover is absent for lighter nuclei, e.g., in the chain of Nd isotopes ($A = 134$–158) explored earlier in Ref. [29]. Probably this is because Nd isotopes do not reach so large a neutron excess as the superheavy elements. Anyway, this turnover of the trend is an interesting feature that deserves further inspection.

C. GDR width and structure: General discussion

In Fig. 11, the isovector dipole strengths calculated with different Lorentz averaging parameters Δ are compared for a representative set of nuclei. It is seen that smaller averaging, $\Delta = 0.5$ and 1 MeV, yields more fine structures, mainly at the resonance peak, and leaves the width almost unchanged. As a rule, $\delta\Gamma = \Gamma(\Delta = 2\ \text{MeV}) - \Gamma(\Delta = 0.5\ \text{MeV}) \leqslant 1$ MeV. Since $\Gamma(\Delta = 2$ MeV) reproduces well the experimental widths, one may associate the difference $\delta\Gamma$ to the smoothing effects omitted in the present RPA calculations (coupling with complex configurations, escape widths). In fact, the averaging with $\Delta = 2$ MeV effectively mimics these effects. Since $\delta\Gamma \ll \Gamma(\Delta = 2\ \text{MeV})$, the deformation splitting and Landau fragmentation (distribution of the collective strength between nearby two-quasiparticle states) obviously dominate the total width. We estimate their contribution to be 70–90%, depending on the nucleus and its shape.

Figure 11 also shows that the averaging $\Delta = 2$ MeV chosen in our calculations is indeed most suitable for the comparison with the GDR experimental data (at least for the heavy nuclei considered here). This averaging does not cause significant artificial increase of the resonance width and, at the same time, allows suppression of the structure details which, in any case, are not resolved in the experimental strength distributions.

Besides the splitting of the GDR into two branches, the deformation also results in a considerable redistribution of the strength within every branch. In other words, the deformation severely influences the Landau fragmentation itself. This effect is illustrated in Table II and Fig. 12. Table II provides the widths of the resonance branches $\mu = 0$ and $\mu = 1$ for a selection of nuclei. There is a large difference between spherical and deformed nuclei. In spherical nuclei (^{304}114, ^{304}120, ^{312}120), we have $\Gamma_0 \approx \Gamma_1 \approx \Gamma$; whereas in deformed nuclei, $\Gamma_1 > \Gamma_0$ and their sum $\Gamma_0 + \Gamma_1$ roughly covers the total width Γ. So, we see a strong deformation effect within the branches themselves. To analyze it, we plot in the lower panels of Fig. 12 the unperturbed two-quasiparticle (2qp) strengths. In deformed

TABLE II. Calculated RPA widths Γ_0 and Γ_1 of the resonance branches $\mu = 0$ and 1, the sum $\Gamma_0 + \Gamma_1$, and the total width Γ. For every nucleus, the deformation parameters β_2 are given. The averaging is $\Delta = 2$ MeV. For more details see the text.

Nucleus	β_2	Widths (MeV)			
		Γ_0	Γ_1	$\Gamma_0 + \Gamma_1$	Γ
^{156}Gd	0.347	3,05	4,74	7,79	7,69
^{172}Yb	0.347	2,54	5,08	7,62	7,28
^{186}Os	0.222	2,65	5,09	7,74	6,39
^{238}U	0.287	2,62	5,11	7,73	6,86
^{254}No	0.308	2,44	5,13	7,57	6,81
^{264}114	0.293	2,74	5,11	7,85	6,47
^{304}114	−0.006	3,98	3,99	7,97	3,98
^{304}120	0.001	3.32	3.26	6.58	3.30
^{312}120	0.038	3,61	3,91	7,52	3,80

nuclei (^{156}Gd), the inequality $\Gamma_1 > \Gamma_0$ appears already in 2qp strengths, which shows that this is simply an effect of the density of states. The residual interaction (SRPA case) does not cause essential changes in the relation between $\mu = 0$ and $\mu = 1$ branches and preserves $\Gamma_1 > \Gamma_0$ in deformed nuclei. Besides showing the influence of deformation, Fig. 12 also illustrates the collective shifts from the unperturbed strengths to the SRPA ones. The size of the shifts is, of course, related to the actual force SLy6. The shifts are 4.0 and 3.4 MeV in ^{156}Gd and ^{304}120, respectively.

For most nuclei, the calculations indicate a small shoulder at the right flank of the resonance. The heavier the nucleus, the stronger the shoulder. At a small smoothing, the shoulder becomes more pronounced and may even show up as a separate peak; see, e.g., results for $\Delta = 0.5$ MeV in Fig. 11. This effect is often absent, or at least much less pronounced, in the experimental data. The shoulder takes place in both deformed and spherical nuclei and so is independent of deformation. It persists not only for SLy6 but also for most other Skyrme forces [25,27]. As shown in Ref. [27], the effect is caused by specific 2qp structures with high angular momentum (thus large statistical weight) lying at the right GDR flank. SRPA neglects some broadening mechanisms (escape widths, coupling with complex, 2p-2h, etc., configurations) which could soften these structures, hence the pronounced effect. The shoulder can be further enhanced if the Skyrme force overestimates the dipole collective shift [25,27]. The case calls for further detailed exploration.

IV. CONCLUSIONS

The isovector giant dipole resonance is systematically investigated in rare-earth, actinide, and superheavy regions. The study covers 37 nuclei altogether. Mainly axially deformed nuclei are considered. In all the nuclei, the calculated quadrupole moments correctly reproduce the experimental data (rare-earth and actinide regions) [45] or macroscopic-microscopic estimates (superheavy region) [41]. The calculations are performed in the framework of the self-consistent separable RPA approach (SRPA) based on the Skyrme functional. The force SLy6 is used.

A satisfying agreement of the SRPA results with the available GDR experimental data is found for 22 rare-earth and actinide nuclei. The trends of the peak energies are compared with simple estimates from collective models. It is confirmed that the Steinwedel-Jensen (SJ) model performs well for medium-heavy nuclei, while a mix of SJ and the Goldhaber-Teller scenarios is more appropriate for heavy nuclei. Encouraged by these results, the survey is extended to superheavy nuclei, where GDR in isotope chains with $Z = 102$, 114, and 120 are explored. The GDR in superheavy nuclei is found to behave similarly to that in rare-earth and actinide nuclei. The peak energies are, again, better described by the mixed collective model, continuing the trend from heavy nuclei. A new feature in the superheavy region is that the peak energies turn from a decreasing trend to an increasing one toward the neutron-rich ends of the isotopic chains (close to the drip lines).

We also analyze the GDR widths Γ. They are shown to be strictly dominated (at least 70–90%) by Landau fragmentation and deformation contributions. The direct deformation contribution through the splitting of the GDR into $\mu = 0$ and 1 branches achieves 40%. The Landau fragmentation is severely affected by the deformation as well, which modifies the branch widths and leads to $\Gamma_1 > \Gamma_0$. The final step to agreement with the experimental pattern is achieved by Lorentz-averaging the SRPA results, thus simulating the missing broadening mechanisms (e.g., escape widths and coupling with complex configurations). A modest additional broadening of $\sim$1 MeV suffices to reach a realistic pattern.

ACKNOWLEDGMENTS

The work was partly supported by DFG Grant RE 322/11-1 and grants from Heisenberg-Landau (Germany, BLTP JINR) and Votruba-Blokhintsev (Czech Republic, BLTP JINR) for 2007 and 2008. W.K. and P.-G.R. are grateful for the BMBF support under Contracts 06 DD 139D and 06 ER 808. This work is also part of the research plan MSM 0021620859 supported by the Ministry of Education of the Czech Republic. It was partly funded by the Czech grant agency (Grant No. 202/06/0363) and grant agency of Charles University, Prague (Grant No. 222/2006/B-FYZ/MFF).

[1] B. L. Berman and S. C. Fultz, Rev. Mod. Phys. **47**, 713 (1975).
[2] A. van der Woude, Prog. Part. Nucl. Phys. **18**, 217 (1987).
[3] K. Langanke and M. Wiescher, Rep. Prog. Phys. **64**, 1657 (2001).
[4] M. Goldhaber and E. Teller, Phys. Rev. **74**, 1046 (1948).
[5] H. Steinwedel and J. H. D. Jensen, Z. Naturforsch. Teil A **5**, 413 (1950).
[6] D. J. Rowe, *Nuclear Collective Motion: Models and Theory* (Methuen, London, 1970).
[7] G. E. Brown, *Unified Theory of Nuclear Models and Forces* (North-Holland, Amsterdam, 1971).
[8] K. Goeke and J. Speth, Annu. Rev. Nucl. Part. Sci. **32**, 65 (1982).
[9] J. Speth and J. Wambach, Int. Rev. Nucl. Phys. **7**, 1 (1990).
[10] G. F. Bertsch and R. A. Broglia, *Oscillations in Finite Quantum Systems* (Cambridge University Press, Cambridge, 1994).
[11] M. Bender, P.-H. Heenen, and P.-G. Reinhard, Rev. Mod. Phys. **75**, 121 (2003).
[12] D. Vretenar, A. V. Afanasjev, G. A. Lalazissis, and P. Ring, Phys. Rep. **409**, 101 (2005).
[13] J. R. Stone and P.-G. Reinhard, Prog. Part. Nucl. Phys. **58**, 587 (2007).
[14] R. M. Dreizler and E. K. U. Gross, *Density Functional Theory* (Springer, Berlin, 1990).
[15] I. Zh. Petkov and M. V. Stoitsov, *Nuclear Density Functional Theory* (Clarendon, Oxford, 1991).
[16] T. H. R. Skyrme, Philos. Mag. **1**, 1043 (1956).
[17] D. Vauterin and D. M. Brink, Phys. Rev. C **5**, 626 (1972).
[18] Y. M. Engel, D. M. Brink, K. Goeke, S. J. Krieger, and D. Vauterin, Nucl. Phys. **A249**, 215 (1975).
[19] S. Shlomo and G. F. Bertsch, Nucl. Phys. **A243**, 507 (1975).

[20] S. Krewald, V. Klemt, J. Speth, and A. Faessler, Nucl. Phys. **A281**, 166 (1977).
[21] P.-G. Reinhard, Ann. Phys. (Leipzig) **1**, 632 (1992).
[22] P.-G. Reinhard, Nucl. Phys. **A649**, 305c (1999).
[23] J. A. Maruhn, P.-G. Reinhard, P. D. Stevenson, J. R. Stone, and M. R. Strayer, Phys. Rev. C **71**, 064328 (2005).
[24] V. O. Nesterenko, J. Kvasil, and P.-G. Reinhard, Phys. Rev. C **66**, 044307 (2002).
[25] V. O. Nesterenko, W. Kleinig, J. Kvasil, P. Vesely, P.-G. Reinhard, and D. S. Dolci, Phys. Rev. C **74**, 064306 (2006).
[26] V. O. Nesterenko, J. Kvasil, W. Kleinig, P.-G. Reinhard, and D. S. Dolci, arXiv:nucl-th/0512045.
[27] V. O. Nesterenko, W. Kleinig, J. Kvasil, P. Vesely, and P.-G. Reinhard, Int. J. Mod. Phys. E **16**, 624 (2007).
[28] V. O. Nesterenko, W. Kleinig, J. Kvasil, P. Vesely, and P.-G. Reinhard, in *Proceedings of the 26th International Workshop on Nuclear Theory, Rila, Bulgaria, 2007*, edited by S. Dimitrova (INRNE BAS, Sofia, 2007), p. 273.
[29] V. O. Nesterenko, W. Kleinig, J. Kvasil, P. Vesely, and P.-G. Reinhard, Int. J. Mod. Phys. E **17**, 89 (2008).
[30] E. Chabanat, P. Bonche, P. Haensel, J. Meyer, and R. Schaeffer, Nucl. Phys. **A635**, 231 (1998).
[31] A. V. Varlamov, V. V. Varlamov, D. S. Rudenko, and M. E. Stepanov, Atlas of Giant Dipole Resonances, INDC(NDS)-394, 1999 (unpublished); JANIS database.
[32] G. M. Gurevich, L. E. Lazareva, V. M. Mazur, S. Yu. Merkulov, G. V. Solodukhov, and V. A. Tyutin, Nucl. Phys. **A351**, 257 (1981).
[33] V. V. Varlamov, M. E. Stepanov, and V. V. Chesnokov, Bull. Russian Acad. Sci. Phys. Ser. **67**, 724 (2003).
[34] B. I. Goryachev, Yu. V. Kuznetsov, V. N. Orlin, N. A. Pozhidaeva, and V. G. Shevchenko, Yad. Fiz. **23**, 1145 (1976).
[35] A. M. Goryachev and G. N. Zalesnyy, Vopr. Teor. Yad. Fiz. **5**, 42 (1976).
[36] A. M. Goryachev and G. N. Zalesnyy, Yad. Fiz. **26**, 465 (1977).
[37] B. L. Berman, D. D. Faul, R. A. Alvarez, P. Meyer, and D. L. Olson, Phys. Rev. C **19**, 1205 (1979).
[38] G. M. Gurevich, L. E. Lazareva, V. M. Mazur, G. V. Dolodovnikov, and B. A. Tulupov, Nucl. Phys. **A273**, 326 (1976).
[39] B. L. Berman, J. T. Caldwell, E. J. Dowdy, S. S. Dietrich, P. Meyer, and R. A. Alvarez, Phys. Rev. C **34**, 2201 (1986).
[40] J. T. Caldwell, E. J. Dowdy, B. L. Berman, R. A. Alvarez, and P. Meyer, Phys. Rev. C **21**, 1215 (1980).
[41] A. Baran, Z. Lojewski, K. Sieja, and M. Kowal, Phys. Rev. C **72**, 044310 (2005).
[42] M. Bender, K. Rutz, P.-G. Reinhard, J. A. Maruhn, and W. Greiner, Phys. Rev. C **60**, 034304 (1999).
[43] M. Bender, W. Nazarewicz, and P.-G. Reinhard, Phys. Lett. **B515**, 42 (2001).
[44] V. V. Varlamov and B. S. Ishkhanov, Part. Nuclei **35**, 859 (2004).
[45] S. Raman, At. Data Nucl. Data Tables **36**, 1 (1987).
[46] M. Brack and W. Stocker, Nucl. Phys. **A406**, 413 (1983).
[47] W. D. Myers, W. J. Swiatecki, T. Kodama, L. J. El-Jaick, and E. R. Hilf, Phys. Rev. C **15**, 2032 (1977).